Available online at www.jpsscientificpublications.com
Volume – 1; Issue - 3; Year – 2015; Page: 228– 235

Indo – Asian Journal of Multidisciplinary Research (IAJMR)
ISSN: 2454-1370

STUDIES ON THE STRUCTURAL, OPTICAL AND ANTIBACTERIAL ACTIVITY OF THE CUO NANOPARTICLES BY SIMPLE CHEMICAL PRECIPITATION METHOD

S. Ramya, G. Viruthagiri*, R. Gobi, N. Shanmugam, N. Kannadasan

Department of Physics, Annamalai University, Annamalai Nagar, Chidambaram 608 002, Tamil Nadu, India.

Abstract

We report the synthesis of copper oxide (CuO) nanoparticles by simple chemical precipitation route using the copper acetate precursor. The synthesized CuO nanoparticles were characterized by X-ray powder diffraction (XRD), the synthesized particles were spherical and particle size was in the range of 24 nm. The Fourier-transform infrared (FTIR) results showed the functional groups required for the reduction of copper ions. UV - DRS is reported from the synthesis CuO nanoparticles and optical results show the bandgap energy (E_g) is 1.94 eV. The photoluminescence spectrum display a broad emission at 527 nm indicates green emission. The morphology of the product was analyzed by field emission scanning electron microscopy (FE-SEM) and confirmed by high resolution transmission electron microscope (HR-TEM) analysis. The magnetic measurements indicated that the obtained CuO nanostructures are found to be room temperature ferromagnetism (RTF). The results reveal that *B. subtilis* shows the maximum inhibition up to 10 mm of the synthesized CuO product.

Key words: CuO nanoparticles, Antibacterial, Optical, FESEM and Oxygen vacancy

1. Introduction

In the last few years the modern society is heavily dependent on semi-conducting metal oxide nanomaterials, which are used in various applications. The nanometer sized alkaline and transition metal oxide materials have recently attracted attention because of their physical and chemical properties (Zhang *et al.*,, 2013). Among, the various transition metal oxides, copper oxide (CuO) are an important p-type transition metal oxide. It is a black solid acting as an electric insulator with a narrow band gap (1.4 eV), which makes it a promising material as semiconductor having high specific capacitances and inexpensiveness, high stability, ease of storage (Rajeshwari *et al.*,, 2014). Copper oxide nanoparticles are used as gas sensors, catalysis, batteries, high temperature superconductors, solar energy conversion tools, etc. (Ren *et al.*, 2009; Hsieh *et al.*, 2003; Zhang *et al.*, 2008). The use of such nanomaterials in medical devices is to prevent bacterial infection (Kumar *et al.*, 2008). Copper (I and II) oxides in their nanoform (<100 nm) displays enhanced antimicrobial activity towards pathogenic microorganisms. Recently many metal oxides such as Ag_2O, ZnO, Fe_2O_3, TiO_2, SnO_2, CeO_2 and polymer membrane composites are known to exhibit good antibacterial activities (Ananth *et al.*, 2015). Numerous reports have been discussed about the antibacterial activities of elemental Cu, CuO and Cu_2O and their related particle size effect,

*Corresponding author: **G. Viruthagiri**
E-mail: gvgiri2002@gmail.com
Received: 30.04.2015; *Revised*: 12.06.2015;
Accepted: 07.07.2015.

morphology and the dissolution of their ions in different medium (Ren *et al.,* 2009; McDonnell *et al.,* 1999; Lu *et al.,* 2009; Meghana *et al.,* 2015). In this present work, an attempt has been made to prepare the CuO nanomaterials by a simple chemical precipitation route. The chemical precipitation route is noted for its simplicity and cost effectiveness for the large-scale production of CuO nanoparticles. The nanoparticles were examined by structural, optical and its application as antibacterial activities.

2. Materials and methods

2.1 Reagents

Copper acetate ($C_4H_6CuO_4.4H_2O$), KOH, absolute ethanol, acetone were of AR grade (99% purity) and used without further purification. Double distilled water was used throughout the experiments.

2.2 Synthesis of CuO nanoparticles

Pure CuO nanoparticles were synthesized by a simple chemical precipitation method. In the preparation of CuO, 0.5 M of copper acetate ($C_4H_6CuO_4.6H_2O$) was dissolved in 50 ml of distilled water and stirred for 15 min. Then 1.5 M of potassium hydroxide (KOH) dissolved in 50 ml of distilled water was added drop wise to the above solution under constant stirring. The obtained blue precipitate of copper hydroxide was stirred and heated at 60 °C until a black precipitate was formed. The obtained precipitate was filtered washed with distilled water and in ethanol several times to remove the impurities. Further, the obtained product was dried in a hot air oven at 100 °C for 7 h. Finally, the obtained products were calcinated at 400 °C for 3 h in a muffle furnace to harvest pure phase of CuO.

2.3 Characterization

The synthesized CuO nanoparticles were characterized by different techniques. The powder X-ray diffraction (XRD) patterns were recorded on an X-ray diffractometer (X'PERTPRO) with monochromated CuKα radiation (λ=1.5406Å). Fourier transform infrared spectrometer (FT-IR) spectra were recorded with a Fourier transform infrared spectrometer (SHIMADZU-8400 FT-IR spectrometer) with KBr pellets in the range of 400-4000 cm^{-1}. Ultraviolet-Visible spectroscopy (UV-Vis) absorption spectra of the samples were recorded on an UV-Vis-NIR spectrometer (Varian/ carry-5000) with a wavelength range of 200-800 nm. The photoluminescence (PL) emission studies of the samples were carried out at a room temperature using Jobin YVON, FLUOROLOG-FL3-11 spectroflurometer. The morphology and size distribution were characterized using FE–SEM (JEOL JSM 6701–F) and TEM measurement in a JEM–2100 instrument. Magnetic measurements were carried out at room temperature using a PMC Micro Mag 3900 model vibrating sample magnetometer (VSM) equipped with 1 T magnet.

Antibacterial activity

Antibacterial activity was screened against four bacterial strains namely Gram –ve bacteria *Pseudomonas aeruginosa*, and *Escherichia coli*, Gram +ve bacteria *Bacillus subtilis* and *Staphylococcus aureus* by Agar well diffusion method (Raja Naika *et al*., 2014). Nutrient Agar plates were prepared and swabbed using Sterile L-shaped glass rod with 100 µl of 24 h mature broth culture of individual bacterial strains. The wells were made by using sterile cork borer (6 mm) wells was created into the each Petri plates. CuO NPs were used to assess the activity of the nanoparticles. The compounds were dispersed in sterile water and it was used as a negative control and simultaneously the standard antibiotics Gentamycin (10 µg/50µl) (Hi Media, Mumbai, India) as positive control were tested against the bacterial pathogens. Then, the plates were incubated at 37 °C for 24 – 36 h, the zone inhibition measured in millimeter (mm) of the every well and also the values were noted.

3. Results and Discussion

3.1 Thermal analysis

In order to ascertain the thermal stability of the as-prepared sample, thermo gravimetric and differential thermal analysis curves were recorded in the temperature range of 30-800 °C in the

nitrogen atmosphere. The obtained curves are shown in Fig. 1. As shown in the figure, the sample shows four stages of weight loss. An initial weight loss of 2.73% recorded between the room temperature, and 130 °C may be ascribed to physisorbed water.

The second stage of a meager weight loss of 1.38% predicted between 130 and 260 °C could be due to the removal of chemisorbed water. A third stage 8.75% weight loss observed between 260 and 310 °C can be pertained to the conversion of Cu $(OH)_2$ into CuO.

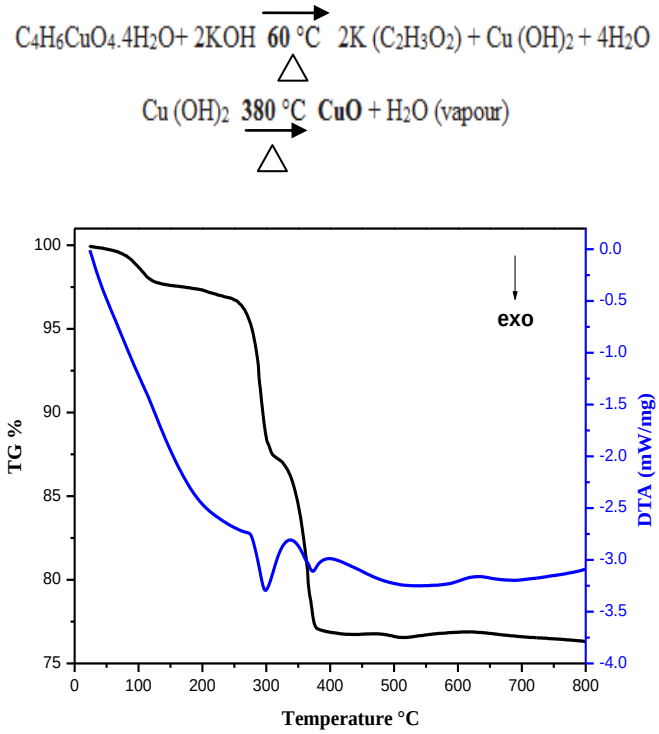

Figure 1: TG - DTA patterns of nanosized CuO

The final weight loss of 10.55% appearing between 310 and 375 °C is due to the crystallization of CuO. Beyond this stage, a further increase of temperature does not affect the thermal stability of the sample as predicted from the plateau region of the curve. The DTA curve with two exothermic peaks at 260°C and 380°C supports the conversion of $Cu(OH)_2$ into CuO and crystallization of CuO, respectively.

3.1 Structural analysis

The crystallographic information of the copper oxide nanoparticles were corroborated by X-ray diffraction (Fig. 2). All the characteristic diffraction peaks show well crystalline distinct monoclinic structure of CuO. X-ray diffraction peaks of the samples are in good agreement with the JCPDS card no. 45-0937 (Mariammal *et al.*, 2013).

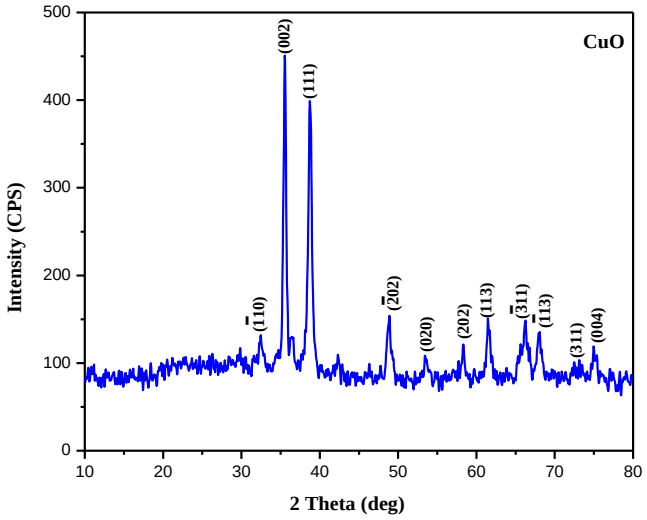

Figure 2: XRD patterns of nanosized CuO

According to the JCPDS card, the synthesized product is a monoclinic phase CuO with cell parameters of a=4.685, b=3.425 and c=5.130 Å and space group of C2/c. All diffraction peaks were only related to CuO without any impurity peaks and thus the synthesized product therefore consist of pure CuO nanoparticles. The average size of CuO nanoparticles (24 nm) were calculated using Scherrer's formula (1) (Kannadasan *et al.*, 2014).

$$D = \frac{K\lambda}{\beta \cos \theta} \qquad (1)$$

Where, D is the crystallite size, K is the Shape factor, λ is the 0.15406 nm, β is the Full width at half maximum, θ is the Reflection angle.

3.3 Optical studies

3.3.1 Ultra Violet-Diffuse reflectance spectrum

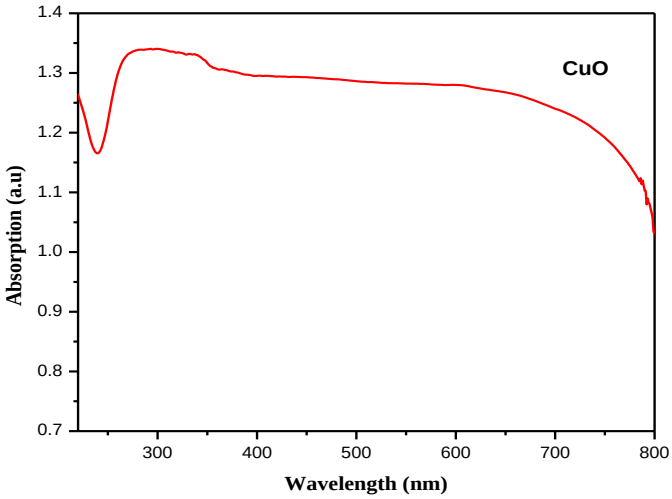

Figure 3: UV–Vis-diffuse reflectance spectrum of CuO nanoparticles

The optical properties of CuO nanoparticles were scrutinized by a UV-Vis spectrum (Fig.3). The room temperature absorption spectrum of pure CuO nanoparticles was recorded in the range of 225-800 nm. The band gap energy (E_g) of pure CuO was obtained from the wavelength value corresponding to the intercept point of the straight line at a=0, which is found to be 638 nm and bandgap energy (E_g) is calculated by using the following equation (2),

$$E_g = \frac{hc}{\lambda}\ eV:\quad E_g = \frac{1240}{\lambda}\ eV \longrightarrow (2)$$

where, Eg is the band gap energy (eV), h is the Planck's constant (6.626 x10^{-34} Js), c is the light velocity (3x10^{8} m/s) and λ is the wavelength (nm). The obtained bandgap energy (E_g) is 1.94 eV.

3.3.2 Photoluminescence (PL) analysis

The Figure 4 shows the PL emission spectrum of pure CuO nanoparticles. A strong photoluminescence was observed at room temperature with the excited wavelength is 500 nm, respectively. The emission band originating from the excited level was monitored in the spectral region between 520 to 550 nm. The energy of the trap level was identified the green emission band at 527 nm is attributed to oxygen vacancies of CuO product (Yang *et al.*, 2008). The green emission band at 525 nm for deep level defects of CuO reported by Jin *et al.* (2010). These oxygen vacancies are allowed to recombine with the photo generated holes and resulted in green emission.

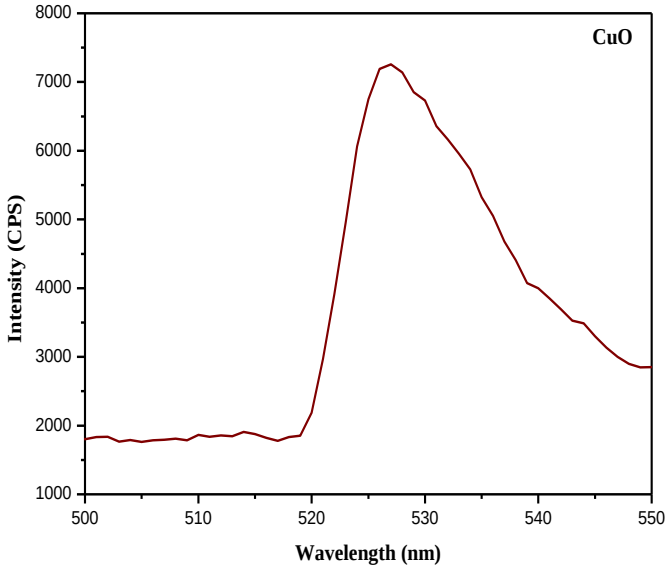

Figure 4: PL spectrum of CuO nanoparticles

3.4 Functional group analysis

The functional group of the CuO nanoparticles was also confirmed by FTIR analysis which was recorded in the range of 4000-400 cm^{-1} and also depicted in Fig. 5. An intense and broad band appeared in the region 3200-3550 cm^{-1} corresponding to the O-H stretching adsorbed water (Nakamoto *et al.*, 1991) which is further confirmed by the band at 1629 cm^{-1}. The band at 2924, 2358 and 1404 cm^{-1} attributed to the stretching vibration of C=H, C=O and C-O bonds respectively. The absorption peaks in the range of 400-850 cm^{-1} are assigned to M-O (M=Cu), O-M-O and M-O-M lattice vibration (Xin-Yao *et al.*, 2012). The very intense band observed at 513 cm^{-1} was assigned to Cu-O bond, (Goswami *et al.*, 2012) respectively.

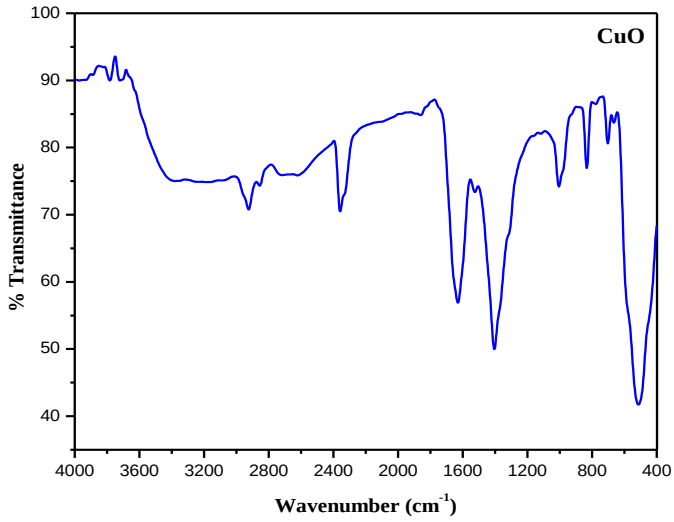

Figure 5: FT-IR spectrum of CuO nanoparticles

3.5 Surface morphological analysis

The morphology surface of pure CuO sample was investigated using FE-SEM. As is seen from Fig. 6(a), the CuO sample is consisted of agglomerated spherical shaped nanoparticles and almost nonuniform morphology, it can be seen that all the nanoparticles are definitely separated with clear boundaries. The CuO exhibited boundary like morphology, the similar results which was reported in the literature (Pendashteh *et al.*, 2013). The bar diagram of quantitative results from EDX analysis undoped sample has been depicted in Fig. 6(b). The result shows the presence of O and Cu are the only elements according to weight % of 27.66 and 72.34 %, respectively. For morphological (size) confirmations, TEM images were recorded for pure CuO.

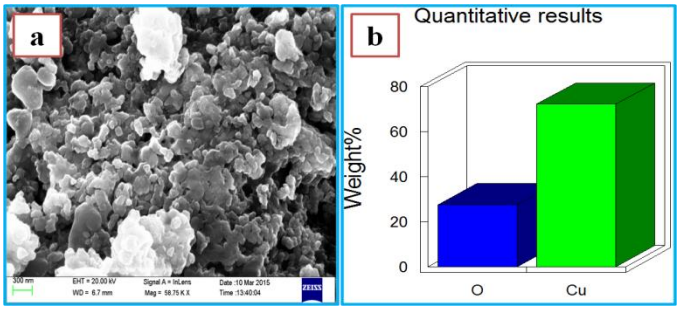

Figure 6: (a) FE-SEM image of CuO nanostructure and (b) bar diagram of quantitative result from EDX analysis

Figure 7(a) shows the aggregated nanoparticles, this is in agreement with the FE-SEM observation. Combine with the TEM images Fig. 7(b), it shows that the continuous lattice fringes with the interplanar spacing of 0.252 nm which are in good agreement with the interplanar distance of (002) plane of the monoclinic structure of CuO. Electron diffraction patterns showed the brightness and intensity of polymorphic discrete ring of the crystalline nanoparticles is shown in Fig. 7(c).

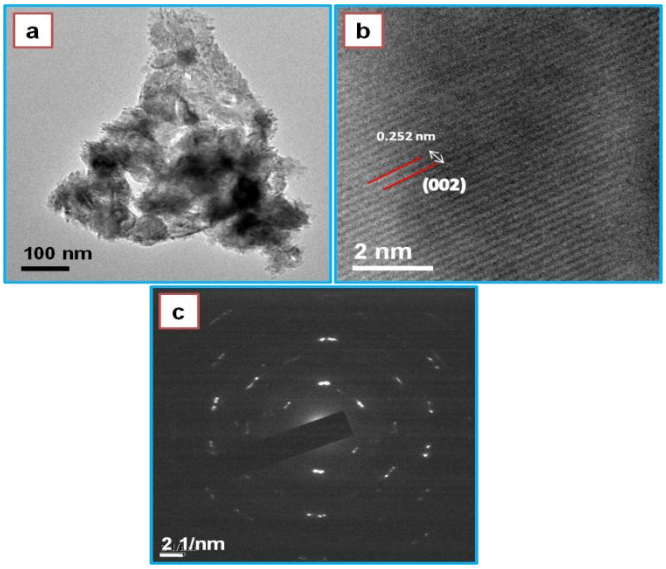

Figure 7: (a) HR-TEM image of CuO nanostructure, (b) Corresponding TEM micrograph and (c) SAED pattern

3.6. Magnetic Study

The effective functioning of the spintronic devices depends on the room temperature ferromagnetism of the semiconductor nanoparticles. Among the metal oxide semiconductors, the P-type conducting nature of CuO finds its applications in the field of gas sensors, superconductors, and solar cells (Mariammal *et al.*, 2013). The magnetic properties of the pure CuO nanocrystals were measured at room temperature by a vibrating sample magnetometer (VSM). Figure 8 shows the dependence of magnetization on the applied magnetic field (M-H curves). It can be seen from Fig. 8 exhibit magnetic hysteresis loops with low

coercivity and high saturation. This indicates the room temperature ferromagnetism of (RTF) CuO.

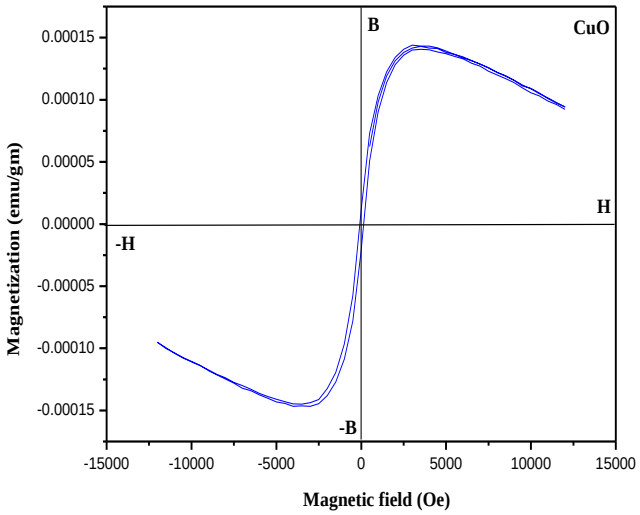

Figure 8: B-H hysteresis loop of CuO nanoparticles

The origin of ferromagnetism is by the presence of the unpaired electrons spin resulting from the oxygen vacancies at the surface/or the interface between the particles and the uncompensated Cu^{2+} ions at the surface (Shang *et al.*, 2009; Zou *et al.*, 2012; Zeng *et al.*, 2009). Gao *et al.*, reported that the oxygen vacancies were a critical factor in introducing RTF in pure CuO nanoparticles (Gao *et al.*, 2010). Zhao *et al.*, presented that RTF observed in pure CuO nanosheets results from the uncompensated spins on the surface (Zhao *et al.*, 2011).

3.7 Antibacterial activity

The antibacterial activity of CuO nanoparticles was investigated both Gram positive (*Staphylococcus aureus* and *Bacillus subtilis*) and Gram negative (*Pseudomonas acruginosa* and *Escherichia coli*) bacteria by zone inhibition methods. The results of zone inhibition method as depicted in Fig. 9. Dasa *et al.* (2013) reported that copper nanoparticles have efficient and bactericidal effect against E. coli and P. aeruginosa. The growth inhibition of cells may be due to distractions of cell membrane by Copper oxide nanoparticles which results in breakdown of cell enzyme (Ren *et al.*, 2009).

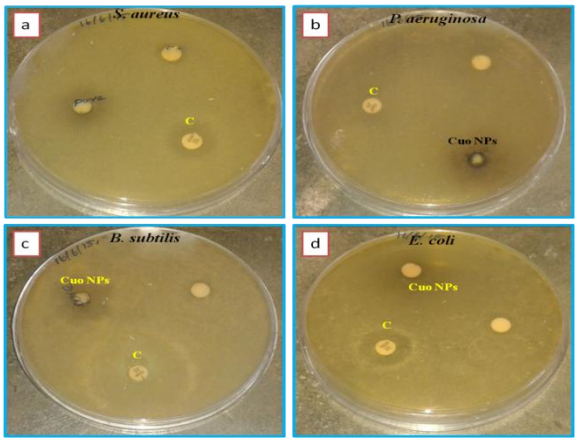

Figure 9: Zone of inhibition of pure CuO nanoparticles (a) *Staphylococcus aureus* (b) *Pseudomonas aeruginosa* (c) *Bacillus subtilis* and (d) *Escherichia coli*

The zone of inhibition values of CuO nanoparticles and standard antibiotic were reported in Table - 1. The results reveal that *B. subtilis* shows the maximum inhibition upto 10 mm followed by *P. aeruginosa* (7 mm), *S. aureus* (7 mm) and *E. coli* (6 mm).

Table - 1: Antibacterial activity of CuO nanoparticles

Microorganisms	Zone of inhibition (mm)	
	Standard control	CuO nanoparticles
P. aeruginosa	10	7
S. aureus	15	7
B. subtilis	15	10
E. coli	12	6

4. Conclusion

Copper oxide nanoparticles were synthesized through a simple chemical precipitation method. The diffraction peaks show monoclinic structured of CuO nanoparticles. The synthesized particles were spherical shape and particle size was in the range of 24 nm. Fourier-transform infrared (FT-IR) results showed the functional group for copper ion is obtained from the absorption band at 513 cm^{-1}. The optical results show the bandgap energy (Eg) is 1.94 eV and broad emission peak at 527 nm shows green emission. The morphology is observed from FE-

SEM and confirmed by HR-TEM. According to the magnetic measurements, an obtained CuO product exhibits the room temperature ferromagnetic behavior. The antibacterial results reveal that *B. subtilis* shows the maximum inhibition up to 10 mm of the prepared CuO product.

Reference

1) Ananth A, Dharaneedharan S, Moon-Soo H and Sun Mok Y. (2015). Copper oxide nanomaterials: Synthesis, characterization and structure-specific antibacterial performance. *Chem. Eng. Journal*, 262:179–188.
2) Dasa D, Bikash Chandra N, Pinkee P and Swapan Kumar D. (2013). Synthesis and evaluation of antioxidant and antibacterial behavior of CuO nanoparticles. *Coll Surf B Biointerfaces*, 101:430 – 433.
3) Gao D, Zhang J, Zhu J, Qi J, Zhang Z, Sui W, Shi H and Xue D. (2010). Vacancy-mediated magnetism in pure copper oxide nanoparticles. *Nanoscale Research Letters*, 5: 769.
4) Goswami A, Raul PK and Purkait MK. (2012). Arsenic adsorption using copper (II) oxide nanoparticles. *Chem Eng Res Design*, 90: 1387 – 1396.
5) Hsieh CT, Chen JM, Lin HH and Shih HC. (2003). Synthesis of well-ordered CuO nanofibers by a self-catalytic growth mechanism. *Applied Physics Letters*, 82(19): 3316 -3318
6) Jin C, Baek K, Park S, Kim HM, Lee WI and Lee C. (2010). Influence of coating and thermal annealing on the structure and luminescence properties of CuO nanorods. *Solid State Communications*, 150: 1812 – 1817.
7) Kannadasan N, Shanmugam N, Cholan S, Sathishkumar K, Viruthagiri G and Poonguzhali R. (2014). The effect of Ce^{4+} incorporation on structural, morphological and photocatalytic characters of ZnO nanoparticles. *Materials Characterization*, 97: 37 – 46.
8) Kumar A, Vemula PK, Aijayan PM and John G. (2008). Silver- nanoparticle-embedded antimicrobial paints based on vegetable oil. *Nat Mater*, 7: 236 – 241.
9) Lu Q, Pang H and Gao F. (2009). Morphology effect on antibacterial activity of cuprous oxide. *Chem Commun*., 1076 – 1078.
10) Mariammal, RN, Ramachandran K, Kalaiselvan G, Arumugam S, Renganathan B and Sastikumar D. (2013). Effect of magnetism on the ethanol sensitivity of undoped and Mn-doped CuO nanoflake. *Appl Surface Science*, 270: 545 – 552.
11) McDonnell G and Russell AD. (1999). Antiseptics and Disinfectants, Activity, Action, and Resistance. *Clin Microbiol Rev*., 12: 147 – 179.
12) Meghana S, Kabra P, Chakraborty S and Padmavathy N. (2015). Understanding the pathway of antibacterial activity of copper oxide nanoparticles. *RSC Adv*., 5: 12293 - 12299.
13) Nakamoto K, Trans D, Huang R, and Wang (Eds.). (1991). Infrared Spectra of Inorganic and Coordination Compound. Chemical Industry Press Beijing 251:4th ed. nanomaterials: Synthesis, characterization and structure-specific antibacterial performance. *Chem Eng J*, 262: 179 – 188.
14) Pendashteh A, Fazlollah Mousavi M and Mohammad Safi R, (2013). Fabrication of anchored copper oxide nanoparticles on graphene oxide nanosheets *via* an electrostatic coprecipitation and its application as super capacitor. *Electrochimica Acta*, 88: 347 – 357.
15) Raja Naika H, Lingaraju K, Manjunath K, Danith Kumar, Nagaraju G, Suresh D and Nagabhushana H. (2014). Green synthesis of CuO nanoparticles using *Gloriosa superba* L. extract and their antibacterial activity. *Journal of Taibah University for Science*, 19(1): 7 - 12.
16) Rajeshwari S, Pattanathu KSM Rahman, Rajiv P, Abdul Salam H and Venckatesh R. (2014). Biogenic copper oxide nanoparticles synthesis using *Tabernaemontana divaricate* leaf extract and its antibacterial activity against urinary tract pathogen. *Spectrochim Acta A*, 133:178–181.

17) Ren G, Hu D, Cheng EWC, Reus MAV, Reip P and Allaker RP. (2009). Characterization of copper oxide nanoparticles for antimicrobial applications. *Int. J Antimicrobial Agents*, 33: 587 – 590.
18) Shang D, Yu K, Zhang Y, Xu J, Wu J, Xu Y, Li L, Zhu Z. (2009). Magnetic and field emission properties of straw-like CuO nanostructures. *Applied Surface Science*, 255: 4093.
19) Xin-Yao Y, Ren-Xia X, Chao G, Tao L, Yong J, Jin-Huai L and Xing-Jiu H. (2012). Novel 3D Hierarchical Cotton-Candy-Like CuO: Surfactant-Free Solvo thermal Synthesis and Application in As(III) Removal. *ACS Appl Mater Interfaces*, 4: 1954 – 1962.
20) Yang Z, Chiang CK and Chang HT. (2008). Synthesis of fluorescent and photovoltaic Cu_2O nanocubes. *Nanotechnology*, 19: 25604 – 25608.
21) Zeng J, Xu J, Tao P and Hua W. (2009). Effect of Fe/Ba mole ratios and surface-active agents on the formation and magnetic properties of co-precipitated barium hexaferrite. *Journal of Alloys and Compounds*, 487: 304.
22) Zhang X, Wang G, Liu X, Wu J, Li M, Gu J, Liu H and Fang B. (2008). Different CuO Nanostructures: Synthesis, Characterization, and Applications for Glucose Sensors. *J Phys Chem*., 112: 16845 – 16849.
23) Zhang Y, Bo X, Nsabimana A, Wang H, Li M and Guo L. (2013)**.** Preparation of copper oxide anchored on surfactant functionalized macroporous carbon composite and its electrochemical applications. *Analyst*, 138: 3633
24) Zhao JG, Liu SJ, Yang SH and Yang SG. (2011). Hydrothermal synthesis and ferromagnetism of CuO nanosheets. *Applied Surface Science*, 257: 9678.
25) Zou CW, Wang J, Liang F, Xie W, Shao LX and Fu DJ. (2012). Large - area aligned CuO nanowires arrays: Synthesis, anomalous ferromagnetic and CO gas sensing properties. *Current Applied Physics*, 12: 1349.